

## THE MASS OF FIRST STARS

HAJIME SUSA<sup>1</sup>Department of Physics, Konan University, Okamoto, Kobe, Japan  
*Draft version November 2, 2018*

## ABSTRACT

We investigate the final mass of the first stars by simulating the gravitational collapse of a primordial gas cloud until  $\sim 0.1$  Myrs after the formation of the primary proto-first-star. According to our numerical experiment using the radiative hydrodynamics calculations, we find that the mass accretions onto the proto-first-stars are significantly suppressed by the radiative feedback from themselves. As a result, we find five stars formed in this particular simulation, and that the final mass of the stars are  $\lesssim 60M_{\odot}$ , including a star of  $4.4M_{\odot}$ . Although it is larger than  $0.8M_{\odot}$ , presence of such a low mass star infer the existence of first stars in the local universe.

*Subject headings:* early universe—HII regions—radiative transfer—first stars

## 1. INTRODUCTION

Formation of the first stars has been investigated intensively in the last decade mainly from theoretical aspects. Following the theoretical predictions, the first stars form in the mini-halos of mass  $\sim 10^5 - 10^6 M_{\odot}$  (Haiman et al. 1996; Tegmark et al. 1997; Nishi & Susa 1999; Fuller & Couchman 2000; Abel, Bryan, Norman 2002; Bromm, Coppi & Larson 2002; Yoshida et al. 2003).

The ingredient of first star formation is the primordial gas, which does not contain heavy elements or cosmic dusts. Because of the lack of these efficient coolants, the primordial gas cools inefficiently especially at low temperatures ( $T \lesssim 10^4\text{K}$ ). Therefore, the gas is kept relatively warm ( $\sim 10^3\text{K}$ ) while it collapses to form stars, in contrast to the case of the interstellar gas, whose temperature is  $\sim 10\text{K}$  during the present-day star formation for  $n_{\text{H}} \lesssim 10^{10}\text{cm}^{-3}$  (e.g. Omukai 2000). As a result, the gravitationally collapsing primordial clouds are very massive  $\sim 1000M_{\odot}$ , since they have to be more massive than the Jean's mass, which is proportional to  $T^{3/2}$ . In addition, formation of such a massive prestellar core leads to huge mass accretion rate onto the protostar in the later mass accretion phase (e.g. Omukai & Nishi 1998; Abel, Bryan, Norman 2002; Yoshida et al. 2006). Following these theoretical evidences, the first stars were once expected to be very massive ( $\gtrsim 100M_{\odot}$ ).

On the other hand, the studies on the mass accretion phase have advanced recently, which revealed that the first star formation process seems to be more complicated than expected before (Clark et al. 2011a,b; Smith et al. 2011; Greif et al. 2011, 2012). They found that a heavy disk formed around the primary protostar, because of the angular momentum of the prestellar core, gained by the tidal interactions with other cosmological overdense regions. The heavy disk fragments into small pieces since it is gravitationally unstable. As a result, a “star cluster” could be formed instead of a single very massive star.

These results seem to be robust until the primary protostar grows to  $\gtrsim 20M_{\odot}$ . After the mass of the protostar exceeds  $\sim 20M_{\odot}$ , significant ultraviolet radiation

flux will be emitted from the protostar (Omukai & Palla 2003; Hosokawa & Omukai 2009; Hosokawa et al. 2011). Thus, the ultraviolet radiation from the protostar significantly affects the later evolution of the system.

Hosokawa et al. (2011) have addressed this feedback effect directly by two dimensional radiation hydrodynamics simulations. They found that the accretion disk around the primary protostar is photoevaporated due to the radiative feedback, followed by the rapid decline of the mass accretion rate onto the protostar. The final mass of the protostar in their simulation is  $43M_{\odot}$ .

Stacy et al. (2012) also tried to assess the final mass of the first stars in their three dimensional cosmological calculations including the fragmentation of the disk as well. They also found that the ultraviolet radiative feedback strongly suppress the mass accretion onto the protostars. However, the integrated physical time is  $\sim 5000\text{yrs}$ , which is too short to predict the final mass of the first stars, since it will take  $\sim 0.1\text{Myrs}$  until the protostar settles onto the main sequence (e.g. Hosokawa & Omukai 2009).

In this paper, we report the results of three dimensional radiation hydrodynamics simulations on the formation of first stars that follow the evolution of the system for  $0.1\text{Myrs}$  after the formation of the primary protostar. We take into consideration the three dimensional effects, as well as the radiative feedback from the protostars.

## 2. NUMERICAL SIMULATION

We study the formation of first stars by radiation hydrodynamics simulations. We employ the Bonner-Ebert sphere of  $n_{\text{H}} = 10^4\text{cm}^{-3}$ ,  $T = 200\text{K}$  as the initial condition of the simulation. This initial condition is motivated by the cosmological simulations (Abel, Bryan, Norman 2002; Yoshida et al. 2003) in which such clouds are found in minihalos of mass  $10^5 - 10^6 M_{\odot}$ , at the “loitering” phase. The loitering phase corresponds to the epoch when the cloud becomes quasi-static, because  $\text{H}_2$  line cooling for  $n_{\text{H}} \gtrsim 10^4\text{cm}^{-3}$  becomes less efficient than that for  $n_{\text{H}} \lesssim 10^4\text{cm}^{-3}$ . In order to make the gas cloud slightly gravitationally unstable, we increase the density by 20%. As a result, the total mass of the cloud is  $2600M_{\odot}$ . We also add uniform rotation to the gas sphere with  $\Omega = 2 \times 10^{-14}\text{rad/s}$ . The angular velocity

<sup>1</sup> susa@konan-u.ac.jp

of this value results in very similar specific angular momentum distribution to that found in the cosmological simulations by Yoshida et al. (2006) at the final stage of the run-away collapse phase.

We use the code Radiation-SPH (Susa & Umemura 2004; Susa 2006) in order to solve the equations of hydrodynamics, non-equilibrium primordial chemistry of six species,  $e^-$ ,  $H^+$ ,  $H$ ,  $H^-$ ,  $H_2^+$ , and radiation transfer of ultraviolet photons. We solve the propagation of Lyman-Werner (LW) band photons as well as the ionizing photons. We use updated self-shielding function for LW radiation transfer (Wolcott-Green et al. 2011). The mass of an SPH particle in the present work is set to be  $m_{\text{SPH}} = 4.96 \times 10^{-3} M_\odot$  and the number of neighbor particles is  $N_{\text{neib}} = 50$ , that correspond to the mass resolution of  $M_{\text{res}} = 2N_{\text{neib}}m_{\text{SPH}} = 0.496 M_\odot$  (Bate & Burkert 1997). This mass resolution is equivalent to the Jeans mass of  $n_H = 10^{12} \text{cm}^{-3}$ ,  $T = 300 \text{K}$ , and comparable to that in Stacy et al. (2012).

In order to trace the evolution in mass accretion phase, we employ sink particles. If the density at an SPH particle exceeds  $n_{\text{sink}} = 3 \times 10^{13} \text{cm}^{-3}$ , we change the SPH particle into a sink particle. In addition, if SPH particles fall within the sphere with radius of  $r_{\text{acc}} = 30 \text{AU}$  centered on a sink particle, and they are gravitationally bound with each other, these SPH particles are merged to the sink particle, conserving the linear momentum and mass. The accretion radius  $r_{\text{acc}}$  is again comparable to that employed in Stacy et al. (2012). We remark that the sink-sink merging is not allowed in the present numerical experiment, since the radius of the protostar is less than  $\sim 1 \text{AU}$  (Hosokawa & Omukai 2009), which is much smaller than the employed accretion radius  $r_{\text{acc}}$ . We regard the mass of the sink particles as the mass of protostars. We also assume that the sink particles do not push surrounding SPH particles, i.e. the pressure forces from sink particles to surrounding SPH particles are omitted. The recipe of sink particles employed in the present work is known to overestimate the mass accretion rate (e.g. Bate et al. 1995; Bromm, Coppi & Larson 2002; Martel et al. 2006). In addition, the employed accretion radius  $r_{\text{acc}} = 30 \text{AU}$ , which is much larger than the radius of protostars (Hosokawa & Omukai 2009). Thus, we have to keep in mind that resultant mass of the formed sink particles would be larger than the actual mass of first stars. We also remark that we cut the central spherical region with radius  $0.6 \text{pc}$  out of the cloud, just after the formation of the first sink in order to save the computational time. The outer envelope of  $r > 0.6 \text{pc}$  hardly affect the inner region within  $10^5 \text{yrs}$ .

The luminosity and the effective temperature of the protostar is obtained by interpolating the results from Hosokawa & Omukai (2009), which are tabulated as functions of protostellar mass ( $M_*$ ) and the mass accretion rate ( $\dot{M}_*$ ).

### 3. RESULTS

We perform radiative hydrodynamics simulations of the first star formation with radiative feedback. We also perform a run with no feedback for comparison.

#### 3.1. Fragmentation of the disk around the primary protostar

We start the simulation from the rigidly rotating Bonner-Ebert sphere around the loitering phase. The cloud starts to collapse in run-away fashion, i.e. the central density keeps growing while the outer part of the cloud is left in the envelope. As a result, density profile of  $\propto r^{-2.2}$  is built up during the run-away phase (Yoshida et al. 2006).

Eventually, the central density exceeds  $n_{\text{sink}}$ , and a sink particle is formed at the center of the cloud. The surrounding gas starts to accrete onto the sink particle subsequently. Since the gas has a significant amount of specific angular momentum, the accreting gas forms an accretion disk around the sink particle. The amount of specific angular momentum in the run-away phase is close to that of the similarity solution, which is approximately 0.5 times the value of Kepler rotation at the Jeans radius, i.e. the core radius (Yoshida et al. 2006). Thus, the radius of the disk is 0.25 times smaller than their original radius at the run-away phase, since the centrifugal force is proportional to the square of the specific angular momentum.

After the formation of the small gas disk around the first sink, the gas keeps accreting onto the disk. As a result, the mass and the radius of the disk increase. At the same time, the temperature of the disk decreases by the radiative cooling. The left column of Fig.1 shows the edge-on views of the disk column density at three epochs corresponding to 320yrs, 620yrs and 860yrs after the formation of the first sink. The red crosses denote the position of sink particles.

In the early epoch of the accretion phase, a smooth disk forms around the sink particle (top panel), followed by the formation of the spiral arms (middle panel) and the fragmentation of the arms (bottom panel). We can also find a few high column density peaks in the bottom panel. In fact, next sink particles are born from these peaks within a few hundred years.

The right column of Fig.1 shows the color contour of Toomre's  $Q$ -parameter, which is given as

$$Q \equiv c_s \Omega_{\text{orb}} / (\pi G \sigma)$$

in case we assume Keplerian motion. Here  $c_s$  denotes the sound velocity of gas,  $\Omega_{\text{orb}}$  is the angular velocity around the central sink particle and  $\sigma$  is the column density of the disk. In the case that the  $Q$ -parameter is less than unity, a smooth disk with density perturbations becomes gravitationally unstable. In fact, the  $Q$ -parameter of the disk at the early phase (top) is already less than unity, so the disk is unstable (middle and bottom).

The time scale of disk fragmentation is given by the linear perturbation theory (Toomre 1964), which is given as  $\Omega_{\text{orb}}^{-1} (Q^{-2} - 1)^{-1/2}$ . The typical value of  $Q$ -parameter in the disk at early phase (top) is  $\sim 0.5$ , and the angular velocity is  $\Omega_{\text{orb}} \simeq 10^{-9} \text{s}^{-1}$ . Thus the perturbation growth time scale is  $\sim 20 \text{yrs}$ , which is comparable to the time scale of the generation of the spiral structure. Thus, spiral structures develop due to the gravitational instability, which could be understood as Toomre's criteria. On the other hand, it takes several hundred years for another sink to be born (bottom), and seemingly via the fragmentation of the spiral arms. Therefore, formation of the sink particles in the disk cannot be understood solely by the simple  $Q$ -parameter argument above, but

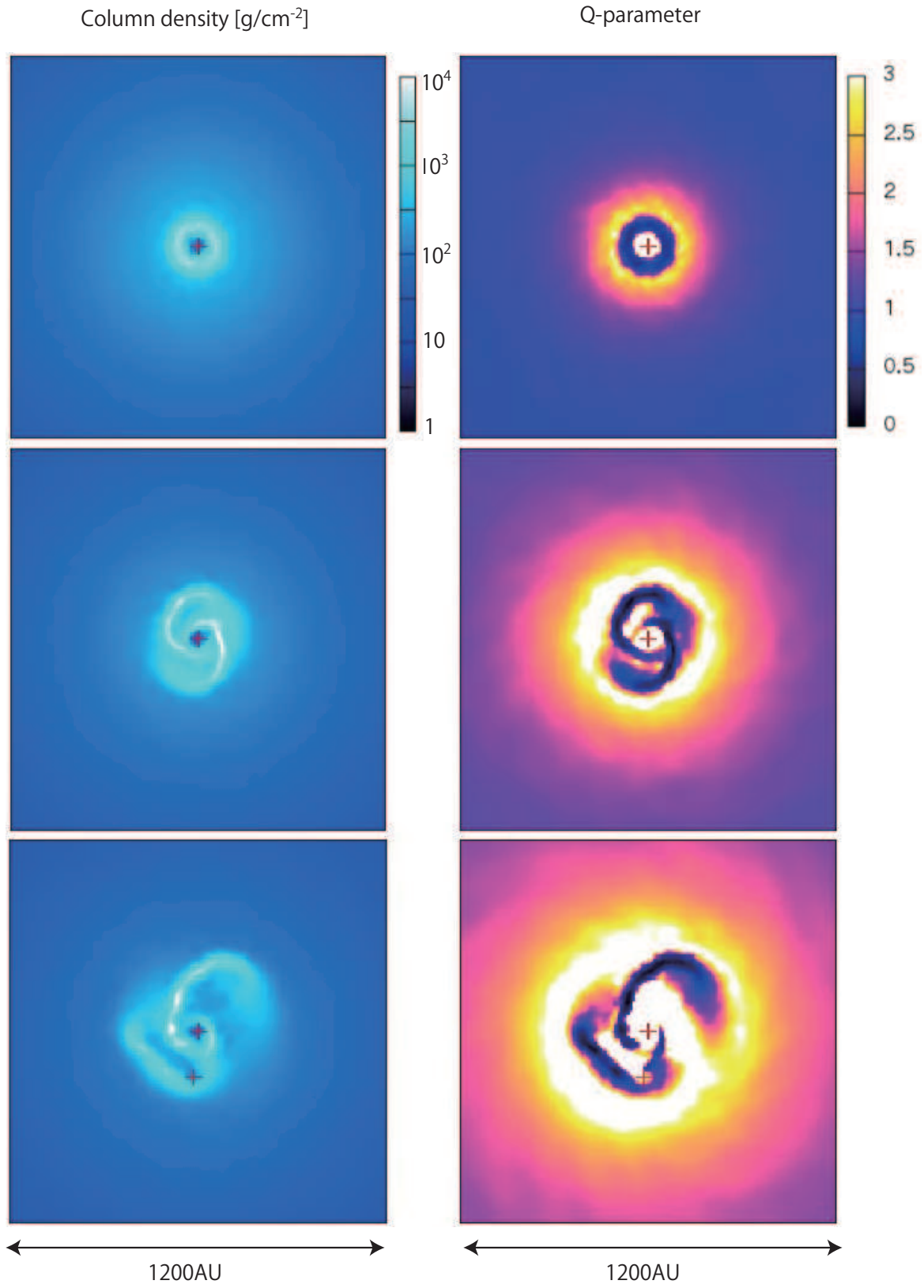


FIG. 1.— Edge-on view at the beginning of the accretion phase. Left column: Three snapshots (320yr, 620yr, 860yr from top to bottom) of color contour of the gas column density. Right column: Toomre's  $Q$ -parameter at the same moment.

requires non-linear calculations.

### 3.2. Effects of radiative feedback

Fig.2 illustrates the evolution of the edge-on view of the central  $10^4\text{AU}$  ( $0.05\text{pc}$ ) in radius. The color shows the fraction of  $\text{H}_2$  molecules, and the transparency denotes the gas density. Small spheres are the position of sink particles. Initially,  $\text{H}_2$  fraction is quite high ( $y_{\text{H}_2} \sim 10^{-2}$ , upper left panel). Eventually, the polar region is photodissociated as the sink particles grow (top right). Some  $\text{H}_2$  rich regions remain along the equatorial plane due to the self-shielding (bottom left), but finally they disappear after  $0.1\text{Myrs}$  (bottom right).

Fig.3 illustrates the evolution of the system on density-temperature plane. Color map shows the frequency distribution of SPH particles on the plane. Four panels show the snapshots at  $t = -10\text{yr}$ ,  $2450\text{yr}$ ,  $5510\text{yr}$ ,  $100250\text{yr}$ , respectively. The distribution of SPH particles on the top left panel is similar to the well known curve of the evolution of collapsing primordial gas in run-away phase (e.g. Palla et al. 1983), since it corresponds to the epoch just before the first sink formation. After the first sink formation, dense gas ( $\gtrsim 10^{10}\text{cm}^{-3}$ ) is splitted to high temperature gas ( $\lesssim 7000\text{K}$ ) and low temperature gas ( $\lesssim 1000\text{K}$ , top right panel). The former corresponds to the radiatively heated gas and the shock heated gas, while the latter is the self-shielded cold gas orbiting around the sink particles. Then, the high temperature gas in the high density region expands due to the increased thermal pressure, generating a shock propagating to low density region (bottom left panel). In fact, we also have seen the shock wave in the bottom left panel of Fig.2, marked by white dashed curve. Finally, the dense cold gas disappears (bottom right), which means that star formation no longer proceeds.

The solid line in Fig.3.2 shows the time evolution of the total mass in the sink particles in the feedback run, whereas the dashed line represents that without radiative feedback effects. It is clear that the mass accretion onto the sink particles is highly suppressed by the radiative feedback. The total sink mass of the run with feedback at the end of the simulation ( $\sim 0.1\text{Myr}$ ) is less than a third of that without feedback. Fig.4 illustrates the time evolution of the mass of the each sink particle. The red curves represent those in the run with the feedback, while the green curves are those results without feedback. In the feedback run, we have one star more massive than  $50M_\odot$  at  $0.1\text{Myr}$  ( $\sim 57M_\odot$ ), whereas we have three stars in the range of  $50 - 200M_\odot$  in the no feedback run.

The minimal sink mass in the feedback run is  $4.4M_\odot$ , and the total number of the sink particles is 5. On the other hand, in the no feedback run, the minimal sink mass is  $0.84M_\odot$ , and the total number of sink particles is 10. It is also worth noting that fragmentation of the disk in the no feedback case continues until much later time ( $\sim 4 \times 10^4\text{yr}$ ) than that in the feedback run ( $\lesssim 1500\text{yr}$ ), because the molecular rich disk is not destoried in the no feedback run. The difference in the number of sink particles and the minimal mass might come from such effect. However, it is premature to draw definitive conclusion on this issue, since our results are based upon only a single realization.

### 3.3. Escapers

In the simulation with feedback, we find a sink particle is kicked away from the central dense region via the gravitational N-body interaction, so-called “slingshot” mechanism. Fig.5 shows the trajectories of all the sink particles within  $(2 \times 10^4\text{AU})^3$  box at the central region. It is clear that one escaping sink goes away from the central region (to the bottom of the panel), whereas the others remain within the box. Such a phenomenon has already been reported by previous groups without radiative feedback effects (e.g. Smith et al. 2011). Thus, we confirm the theoretical existence of such escapers also in our numerical model with radiative feedback. The velocity of this escaping sink is  $\sim 4\text{km/s}$  at  $0.1\text{pc}$  distant from the center of the cloud, which is marginal to escape from the host minihalo of  $10^6M_\odot$ .

The mass accretion onto this escaping particle almost stops after the ejection. Consequently, the mass of the sink is  $4.4M_\odot$ , that are much smaller than the “conventional” first stars of mass  $\gtrsim 100M_\odot$ . It is also worth noting that the orbit of the other sinks are excited by the N-body interaction with each other, although they are not ejected. Thus, some of the sinks going through relatively low density regions, which results in low mass accretion rate onto these sinks.

We also remark that a star less massive than  $0.8M_\odot$  is found in our higher resolution run ( $M_{\text{res}} = 0.1M_\odot$ ) with feedback, although the integrated physical time is  $\sim 2 \times 10^4\text{yrs}$  (Umemura et al. 2012). Considering the fact that the mass resolution and the accretion radius of the present simulations are  $\sim 0.5M_\odot$  and  $30\text{AU}$ , and other higher resolution studies with/without feedback effects report the ejection of even lower mass stars (Umemura et al. 2012; Clark et al. 2011a,b; Smith et al. 2011; Greif et al. 2011, 2012), we presume that low mass stars less massive than  $0.8M_\odot$  are born among the first stars, and survive through the entire history of the universe.

## 4. DISCUSSIONS

In the presence of radiative feedback, the gas in the neighborhood of protostars is heated up significantly. This heating process occurs mainly through photodissociation of  $\text{H}_2$  molecules: Formation of  $\text{H}_2$  molecules works as a heating process of the gas, since formation process such as  $3\text{H} \rightarrow \text{H}_2 + \text{H}$  or  $\text{H}^- + \text{H} \rightarrow \text{H}_2 + \text{e}^-$  releases the latent heat. In the absence of radiative dissociation process, collisional dissociation processes absorb thermal energy, which balance with the formation heating. Thus, the net increase of  $\text{H}_2$  molecules causes effective heating of the gas, while the net decrease of  $\text{H}_2$  results in cooling. On the other hand, in the presence of strong photodissociative radiation, it overwhelms other collisional dissociation processes. The photodissociation process do not absorb thermal energy, since the energy required to dissociate  $\text{H}_2$  molecules is supplied by the radiation. Therefore,  $\text{H}_2$  dissociation is no longer a cooling process. As a result,  $\text{H}_2$  formation heating proceeds without hinderance in the absence of the counter process.

In fact, Fig.6 illustrates the ratio between the  $\text{H}_2$  formation heating rate and the adiabatic heating rate as functions of gas temperature and density at  $t = 2450\text{yr}$ . It is clear that  $\text{H}_2$  formation heating is the dominant

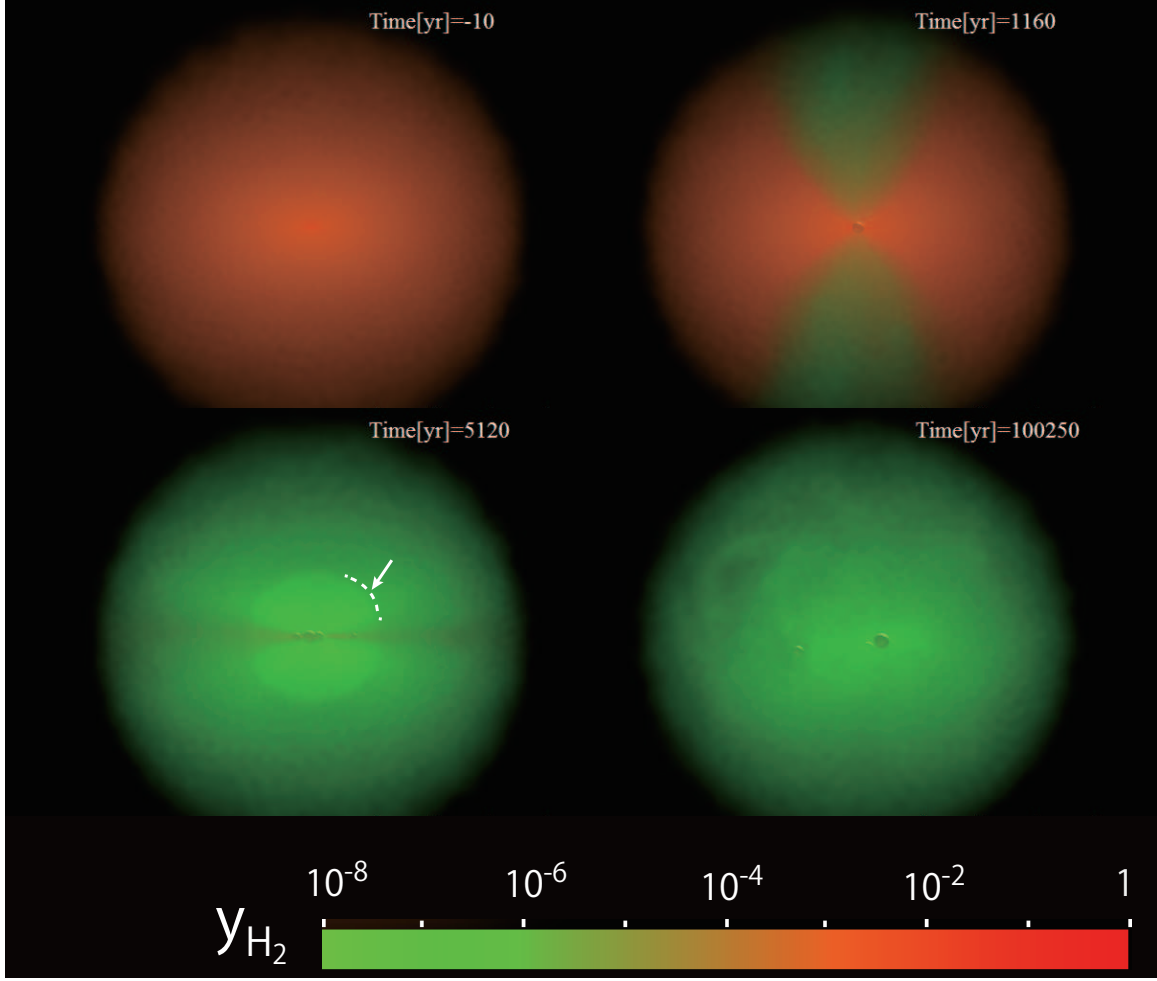


FIG. 2.— Edge-on views of gas distribution inside  $r < 10^4$  AU (0.05 pc) at four snapshots. Left column: from top to bottom,  $t = -10$  yr, 1160 yr. Right column:  $t = 5120$  yr, 100250 yr.  $t$  represents the time after the first sink formation. Color shows the  $H_2$  fraction, and the small spheres represent the positions of sink particles. White arrow and dashed curve in the top right panel denotes the position of the shock front.

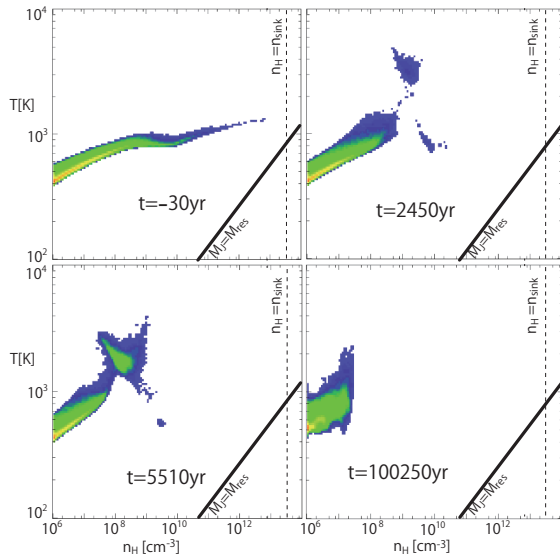
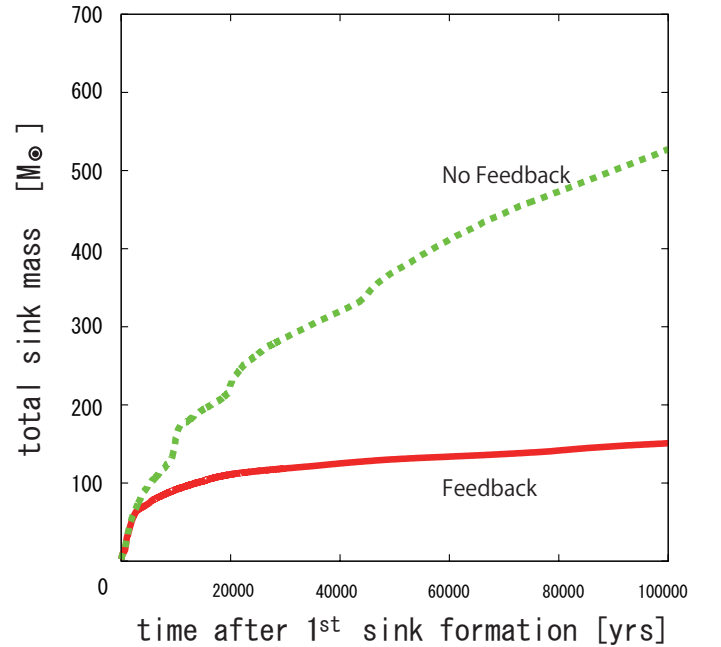


FIG. 3.— Four snapshots on the density-temperature plane. Color represents the number of SPH particles drop on the logarithmic bin on the plane. Thick solid lines show the resolution limit of this simulation, while dashed lines represent the number density above which the SPH particles are converted to sink particles.



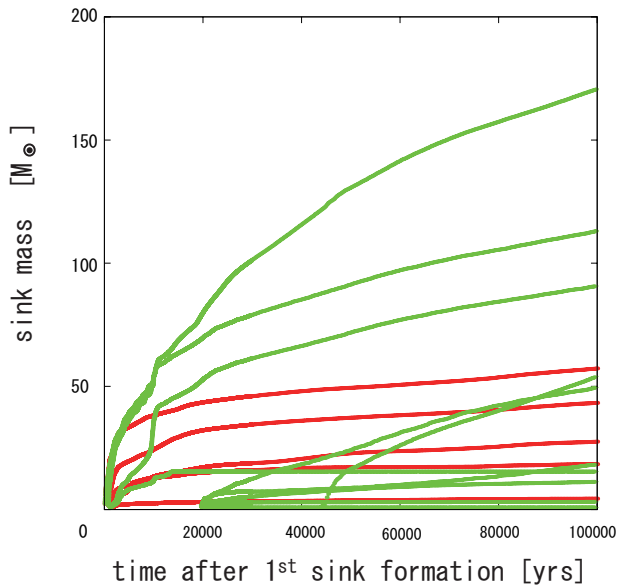


FIG. 4.— The mass of individual sink particles are plotted as functions of time after the first sink formation. Red curves for the runs with feedback, while the green curves for the case without feedback.

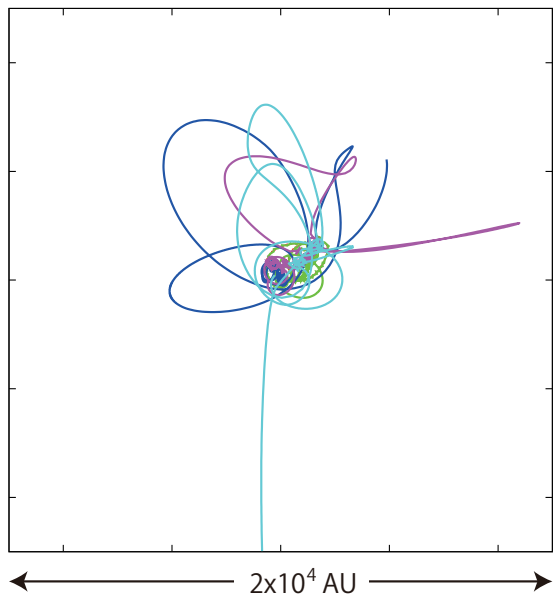


FIG. 5.— The trajectories of sink particles in edge-on view.

heating process at high densities ( $n_H \gtrsim 10^{10} \text{cm}^{-3}$ , right panel). The temperature of these chemo-heated high density regions is mainly around 1000K, and the chemical heating is also important for high temperature region at  $3000\text{K} \lesssim T \lesssim 7000\text{K}$  (left panel). It is also clear that chemical heating rate is not negligible compared to the adiabatic heating rate even at lower densities ( $\sim 10^6 \text{cm}^{-3}$ ) and lower temperatures ( $T \sim 300\text{K}$ ), which corresponds to the dissociated polar regions. Thus, chemical heating of  $\text{H}_2$  formation play important roles on the dynamical evolution of this system.

Heating through photoionization is also important. In fact, similar calculation in 2D by Hosokawa et al. (2011), photoionization is the dominant heating process. They found that gas in the polar region is highly ionized and

heated up to  $> 10^4\text{K}$ . Finally, the disk is photoevaporated mainly due to the photoheating process through ionization. In the present calculation, however, ionization is not the dominant heating process. The reason simply comes from the fact that the spatial resolution of the present simulation is not enough to resolve the “initial” Strömgren sphere (Spitzer 1978). The SPH particles in the very vicinity of the source star is heated by ionization only “mildly”,  $T \lesssim 10^4\text{K}$ , which cannot cause the drastic propagation of D-type ionization front which is found in Hosokawa et al. (2011). In other words, this radiative feedback effect is underestimated in the present simulation.

As noticed in section 2, the algorithm of mass accretion onto sink particles overestimates the mass accretion rate. Combined with the fact that feedback is underestimated, the mass accretion rate obtained in the present numerical experiment is overestimated at any hand. Accordingly, the final mass of the sinks should be regarded as an upper limit of the actual mass of first stars. If we could perform simulations at higher resolution with more realistic mass accretion conditions, the final mass could be smaller than  $\sim 50M_\odot$ . We also should keep in mind that this result comes from a numerical experiment of one realization. Thus, this upper limit should be regarded as a guide, since a slightly different initial condition could cause different result because of the chaotic nature of the system. In any case, the final mass of the sinks seem not to exceed  $100M_\odot$  from typical initial conditions. On the other hand, at least one of the protostars cannot be less massive than  $M \sim 20M_\odot$ , since the radiative feedback becomes prominent only for  $M_* \gtrsim 20M_\odot$ . Thus, the mass of the primary star among the first stars formed in a single mini-halo will fall in the range of  $20 - 60M_\odot$ .

The initial condition of the present experiment is a rigidly rotating Bonner-Ebert sphere. Although its angular momentum distribution just before the sink formation is close to that of cosmological simulations, it is not fully cosmological. In cosmological simulations, the direction of angular momentum of the disk around the primary protostar changes depending on the stages, since the gas motion is more turbulent. In addition, we need more numerical experiments starting from various initial conditions, in order to obtain statistical quantities such as the initial mass function (IMF) of first stars. Thus it is important to perform fully cosmological simulations of this sort, which is left for future works.

## 5. SUMMARY

In this paper, we investigated the suppression of mass accretion onto proto-first-stars by the radiative feedback from themselves. We performed numerical experiment of the formation of first stars using three dimensional radiative hydrodynamics code RSPH combined with sink particle technique. Consequently, we find that the mass accretion is suppressed significantly and the final outcome is a multiple stellar system consisting of five stars of  $1 - 60M_\odot$ . The fact that low mass stars are found in this work infer the possible existence of first stars in the local universe, although the mass of the formed stars in our simulation is still larger than  $0.8 M_\odot$ .

We thank T. Hosokawa for providing the data of proto-first-stars. We also thank K. Omukai for careful reading



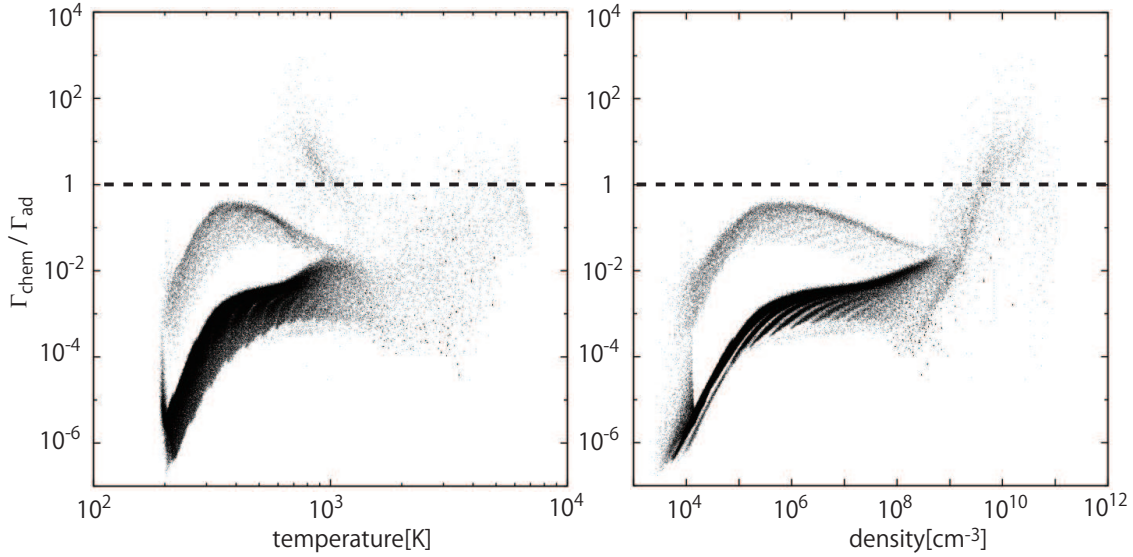


FIG. 6.— The ratio between the chemical heating rate and the adiabatic heating rate is plotted as functions of temperature (left panel) and density (right panel) at  $t = 2450$ yr.

of the manuscript. This work was supported by Ministry

of Education, Science, Sports and Culture, Grant-in-Aid for Scientific Research (C), 22540295.

#### REFERENCES

- Abel, T., Bryan, G. L., & Norman, M. L. 2002, *Science*, 295, 93  
 Bate, M. R., Bonnell, I. A., & Price, N. M. 1995, *MNRAS*, 277, 362  
 Bate, M. R., & Burkert, A. 1997, *MNRAS*, 288, 1060  
 Bromm, V., Coppi, P. S., & Larson, R. B. 2002, *ApJ*, 564, 23  
 Clark, P. C., Glover, S. C. O., Smith, R. J., et al. 2011, *Science*, 331, 1040  
 Clark, P. C., Glover, S. C. O., Klessen, R. S., & Bromm, V. 2011, *ApJ*, 727, 110  
 Fuller, T. M., & Couchman, H. M. P. 2000, *ApJ*, 544, 6  
 Greif, T. H., Bromm, V., Clark, P. C., et al. 2012, *MNRAS*, 424, 399  
 Greif, T. H., Springel, V., White, S. D. M., et al. 2011, *ApJ*, 737, 75  
 Haiman, Z., Thoul, A. A., & Loeb, A. 1996, *ApJ*, 464, 523  
 Hosokawa, T., & Omukai, K. 2009, *ApJ*, 691, 823  
 Hosokawa, T., Omukai, K., Yoshida, N., & Yorke, H. W. 2011, *Science*, 334, 1250  
 Martel, H., Evans, N. J., II, & Shapiro, P. R. 2006, *ApJS*, 163, 122  
 Nishi, R., & Susa, H. 1999, *ApJ*, 523, L103  
 Omukai, K. 2000, *ApJ*, 534, 809  
 Omukai, K., & Nishi, R. 1998, *ApJ*, 508, 141  
 Omukai, K., & Palla, F. 2003, *ApJ*, 589, 677  
 Palla, F., Salpeter, E. E., & Stahler, S. W. 1983, *ApJ*, 271, 632  
 Smith, R. J., Glover, S. C. O., Clark, P. C., Greif, T., & Klessen, R. S. 2011, *MNRAS*, 414, 3633  
 Spitzer, L. 1978, New York Wiley-Interscience, 1978. 333 p.249  
 Stacy, A., Greif, T. H., & Bromm, V. 2012, *MNRAS*, 422, 290  
 Susa, H. 2006, *PASJ*, 58, 445  
 Susa, H., & Umemura, M. 2004, *ApJ*, 600, 1  
 Tegmark, M., Silk, J., Rees, M. J., et al. 1997, *ApJ*, 474, 1  
 Toomre, A. 1964, *ApJ*, 139, 1217  
 Umemura, M., Susa, H., Hasegawa, K., Suwa, T., & Semelin, B. 2012, *Prog. Theor. Exp. Phys.*, 01A306  
 Wolcott-Green, J., Haiman, Z., & Bryan, G. L. 2011, *MNRAS*, 418, 838  
 Yoshida, N., Abel, T., Hernquist, L. & Sugiyama, N., 2003, *ApJ*, 592, 645  
 Yoshida, N., Omukai, K., Hernquist, L., & Abel, T. 2006, *ApJ*, 652, 6